I&EC research
Industrial & Engineering Chemistry Research

Article

pubs.acs.org/IECR

Review: Photochemical and Thermochemical Production of Solar Fuels from H_2O and CO_2 Using Metal Oxide Catalysts

Greg P. Smestad*,† and Aldo Steinfeld‡,§

†Solar Energy Materials & Solar Cells, P.O. Box 5729, San José, California 95150, United States
‡Department of Mechanical and Process Engineering, ETH Zürich, 8092 Zürich, Switzerland
§Solar Technology Laboratory, Paul Scherrer Institute, 5232 Villigen PSI, Switzerland

ABSTRACT: Metal oxides are reviewed as catalysts to convert H_2O and CO_2 to fuels using solar energy. For photochemical conversion, TiO_2 has been found to be the most stable and useful oxide material, but it is currently limited by its large bandgap and a mismatch between its conduction band and the redox couples for water splitting and CO_2 reduction. A theoretical framework has been utilized to understand the basic thermodynamics and energetics in photochemical energy conversion systems. This is applied to model systems comprised of Ag_2O and AgCl to examine why the former reacts thermochemically in air, while the latter reacts photochemically. For thermochemical conversion, zinc-, ceria-, and ferrite-based redox cycles are examined and examples of high-temperature solar reactors driven by concentrated solar radiation are presented. For CO_2 splitting, theoretical solar-to-fuel energy conversion efficiencies can be up to 26.8% for photochemical systems, and can exceed 30% for thermochemical systems, provided that sensible heat is recovered between the redox steps.

INTRODUCTION

The conversion of solar energy into useful forms has reached a critical stage where large-scale industrial applications are allowing it to make significant and promising contributions to our present and future energy needs. In this review, we present some basic concepts and survey a few of the recent developments in the conversion of solar energy into fuel. Several types of systems are possible, some of which are based on thermochemistry,[1] while others are based on photochemistry.[2] Photovoltaic cells and modules[3−7] have also emerged as an important part of the energy mixture of many countries, but they will not be fully examined in this review. The storage of solar energy has recently been reported in this journal.[8] The first section of this review focuses on the photochemical production of fuels and includes a generalized framework that can be used to understand the energetics and mechanism of both photovoltaic (PV) solar cells, as well as solar photochemistry using semiconductor materials.[9−12] This framework will be applied to a consideration of Ag_2O, which is a model metal oxide system that, in air, seems to react thermochemically but not photochemically. The second half of this review focuses on the solar thermochemical splitting of H_2O and CO_2 via metal oxide redox cycles. A comparison between metal oxide and solar electrolysis fuel-forming systems will also be presented.

DISCUSSION

Photochemistry and Quantum Solar Converters. Two forms of solar energy conversion are considered. One is thermal conversion, where work can be extracted after sunlight is absorbed as thermal energy, and the other is quantum conversion, where the work output can be taken directly from the light absorber. In a thermal system, solar radiation is absorbed as heat, preferably at some high temperature, which, in turn, is used to drive a heat engine. In a quantum system, a fixed number of photons yield a fixed number of energy quanta, such as excited electrons. Photochemistry therefore differs from thermochemistry in that the former involves the energy of a photon in a chemical reaction, while the latter involves the absorption of heat to overcome activation barriers and affect chemical equillibria. Solar photochemistry utilizes concepts in quantum solar energy conversion that stem from the consideration of the excited state that is produced via the absorption of light. The light absorber can be a semiconductor, a molecule, or an organic compound. The photon-induced excitation may produce work, or it may decay to dissipate the excitation energy as heat or light (i.e., luminescence). Regarding the latter, if the interaction of light with a light absorber material produces electrons, or a species in a higher energetic state, then the reverse process, which must also be possible, will produce light emission from the material.[13] This is the definition of photoluminescence, which is present, to some degree, in all quantum solar converters.

Many researchers have used these concepts and applied detailed balance calculations to understand the thermodynamic limits of quantum solar converters such as photochemical energy storage systems and photovoltaic solar cells.[13−24] For photochemical solar conversion and storage systems, the work of Ross[15,25−27] was groundbreaking, as was the early work of Archer and Bolton.[16] These detailed balance studies have continued up to the present time and are especially useful in studying PV solar cells, photosynthetic bacterial reaction centers, and photochemical energy conversion. Recent results

Special Issue: Alternative Energy Systems

Received: March 25, 2012
Revised: May 29, 2012
Accepted: May 31, 2012
Published: May 31, 2012

show that, for the standard solar spectrum (AM1.5), theoretical energy conversion efficiencies can be up to 26.8% for photochemical systems.[17] This compares favorably with the ideal limit for solar cells (30%−33%) and the measured efficiency for silicon solar cells, which are now in the range of 15%−24%.[6,7] In a solar cell, the excitation takes the form of an electron−hole pair that is separated in order to produce an external current and voltage. In photosynthesis, the spatially separated electrons may reduce compounds that lead to the fixation of CO_2 and to the storage of biomass that can be used as food and fuel. With so many varied quantum solar converter systems in the literature, it is useful to briefly consider a generalized model that can be used to inter-relate and discuss recent results.

Thermodynamics and Quantum Solar Converters. A general solar quantum converter scheme is shown in Figure 1.[16,20] The light absorber functions as a "pump" to move

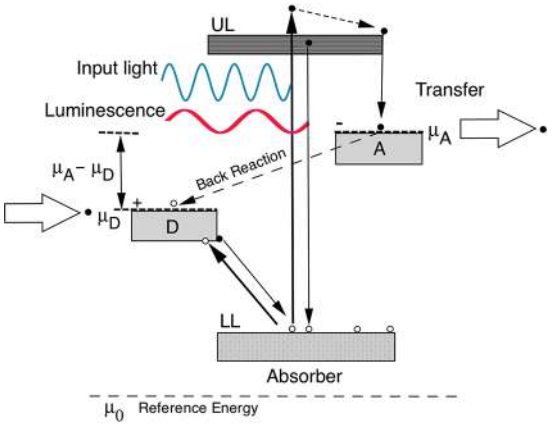

Figure 1. Generalized solar converter applicable to both photochemical systems, including photosynthesis and solar cells (photovoltaics). The absorber pumps electrons from a donor (D) to an acceptor (A) via lower and upper levels (LL and UL, respectively). This allows a difference to develop between the concentration of excited states on the two sides of a barrier. Work can be produced when the electrons and holes are extracted (horizontal arrows). Radiative and nonradiative recombination competes with work extraction. The difference in chemical potentials (μ) is indicated.

electrons and holes between the two sides separated by an interface or barrier. Back reaction, as well as nonradiative recombination and luminescence, compete with energy conversion and work production (shown as horizontal arrows). This is given by the difference between the chemical potentials of electrons and holes on the two sides of the converter ($\mu_A - \mu_D$). This is maintained by the pump, due to its ability to maintain a difference between the concentration of excited electrons and holes on the acceptor and donor sides of the interface. The concentration of electrons is n_A and n_D on the acceptor (subscript A) and donor (subscript D) sides of the interface, and the concentration of holes is p_A and p_D on the acceptor (subscript A) and donor (subscript D) sides of the interface. The equilibrium concentrations in the dark are given by n_0 and p_0, and under illumination, they are limited to the initial excited state populations, n^* and p^*.[16,27] At an ambient temperature T_0, the rate of work extraction (i.e., the rate of energy conversion or power output) is then given by the difference in chemical potentials multiplied by the rate of photoproduct production, $\dot{n}$, and is given by

$$\dot{n}(\mu_A - \mu_D) = \dot{n}kT_0 \ln\left(\frac{n_A p_A}{n_D p_D}\right) \leq \dot{n}kT_0 \ln\left(\frac{n^* p^*}{n_0 p_0}\right) \quad (1a)$$

where k is Boltzmann's constant. This equation reflects the view that quantum solar conversion can be treated like a chemical reaction involving the exchange of chemical potential, or Gibbs free energy, between the incident photons and the excited state of the electrons and holes.[13] The photoproduct can be electrons and holes for a solar cell, or these species can go on to produce reduced and oxidized products in photochemical or electrochemical reactions. If q is the charge on an electron, $\mu = qV$ and $\dot{n}q = I$ (i.e., the electrical current). We then have, for the case of a solar cell, that the left-hand side of eq 1a becomes the current multiplied by the voltage at the terminals of the device.

For a time-symmetric quantum solar conversion system, one can also demonstrate that if entropy production is the minimum allowed by thermodynamics, the power production (i.e., the rate of work extraction) will be maximized. Using the concepts of irreversible and finite-time thermodynamics, it has been shown[28,29] that the maximum rate of work extraction in any power converting system is given by the reversible work production rate ($\dot{W}_{rev}$) minus the product of the total entropy generation rate ($\dot{S}_{tot}$) and the temperature (T_0). The former is described by a Carnot-type factor, while the latter defines the dissipation of available work. Starting with the generalized Planck equation,[14] and using the entropy involved in the absorption and emission of light, Parrot,[18] as well as Markvart and Landsberg,[20] have derived an equation for a quantum solar converter of the same form as that obtained by Berry and coworkers.[28,29] Combining the results from these authors, one obtains

$$\dot{n}(\mu_A - \mu_D) = \dot{W}_{rev} - T_0\dot{S}_{tot} = P_{abs}^{net}\left(1 - \frac{T_0}{T_S}\right) - \text{dissipation} \quad (1b)$$

where the net power absorbed in the photoconverter is P_{abs}^{net}. The converter temperature is T_0, and the source temperature (i.e., the sun) is T_S. These equations illustrate that a quantum solar converter, such as a solar cell or photochemical converter, maintains a nonequilibrium state from which work can be extracted if entropy production does not dissipate the spatial differences between electrons and holes. Not explicitly shown in Figure 1 are the important interface and defect states that may dissipate energy via nonradiative recombination. The equations and approach above are called "general" or "generalized", because they apply to quantum solar converters, regardless of the specific details or design of the system.

With this general framework in mind, the topic of thermochemical reduction of metal oxides will be introduced, using the example of silver oxide. This will be compared and contrasted with silver chloride, which reacts photochemically to form reduced silver. Figure 1 and the concepts surrounding eqs 1a and 1b will then be utilized to examine the results for these materials and review some recent results using metal oxides for the photochemical conversion of solar energy. Finally, several promising thermochemical systems will be described and such systems will be compared to photochemical schemes and solar fuel production methods using solar-generated electricity coupled to an electrolyzer.

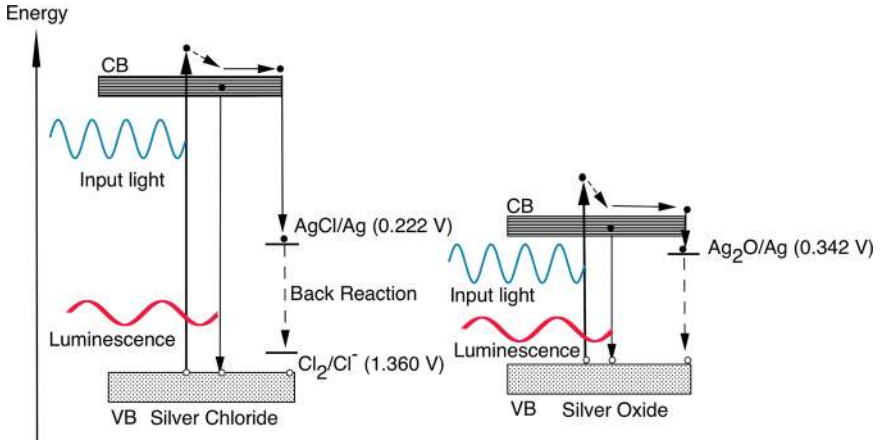

Figure 2. Band diagram for AgCl (left) and Ag_2O (right) showing electron excitation and trapping to form reduced silver. Standard redox potentials vs NHE are displayed in parentheses for reference. The CB edge for Ag_2O was taken from the literature for the oxide in aqueous solution.[33,42].

Silver Oxide and Silver Chloride: Thermochemistry and Photochemistry. Silver oxide and alkali halide-based photocathodes are commonly used in photodetectors and photomultipliers.[30] As shown in previous work, these materials can simultaneously convert heat and light into electrical work when they are utilized as photocathodes in thermionic diodes.[31] This may also be possible using a suitable photochemical reaction. This would be desirable, since the storage of solar energy could be more efficiently achieved. An S1 photocathode[30,32] comprised of Ag_2O:Cs was used in vacuum phototube experiments to learn that photoexcited electrons can produce electrical work concurrently with thermionic conversion.[31] Recently, Ag_2O has been found to be a stable photocatalyst in aqueous solution.[33] It is unstable under visible-light irradiation and decomposes into metallic Ag during the photocatalytic decomposition of organic substances. However, after partial formation of reduced Ag in situ on the surface of the Ag_2O/Ag composite, it can function as a more stable and efficient visible-light photocatalyst. In light of this new result, and in preparation for the review of results on the thermochemical reduction of metal oxides by concentrated sunlight, it is therefore useful to examine some results regarding this oxide and compare it to AgCl.

Semiconductors Ag_2O and AgCl may produce reduced Ag atoms with the release of gaseous oxygen (O_2) and chlorine (Cl_2), respectively.[34−41] Before the advent of digital photography, silver chloride (with a bandgap of ∼3 eV) was widely utilized, together with organic sensitizers, to extend its light absorption into the visible range.[39,43] During the recording process, photoexcited electrons produce reduced silver and gaseous chlorine. In air, silver oxide (Ag_2O, with a bandgap of 1.3 ± 0.1 eV) undergoes thermal decomposition and silver reduction at temperatures in the range of 250−400 °C.[36,37] The energy band diagram for these two binary silver compounds is shown in Figure 2, together with the literature values of the standard redox potentials for the reduction reactions[33,35,38,39,42] at room temperature. Both of these compounds are known to exhibit photoluminescence.[34] In addition, AgCl is known to produce voltages of >1 V in photoelectrochemical (PEC) cells and exhibit Ag reduction, utilizing a two-step (defect-mediated) mechanism.[40,41] It is therefore instructive to ask whether both thermochemical and photochemical reduction reactions can occur at the same time within the framework of Figure 1.

For the process in Figure 2, the thermal decomposition reaction Ag_2O can be envisioned as the following reduction:

$$Ag_2O + H_2O + 2e^- \rightleftharpoons 2Ag + 2OH^- \qquad E^0 = +0.342\ V \tag{2}$$

$$Ag_2O \overset{heat}{\rightleftharpoons} 2Ag + \frac{1}{2}O_2 \tag{3}$$

It is reasonable to believe that reaction 2 occurs in aqueous environments, or in the presence of moisture.[33] The corresponding half-reaction for the oxidation may be O_2/OH^- (0.401 V), but several other reactions involving water and oxygen are also possible.[42] At elevated temperatures in air or vacuum, the mechanism for reaction 3 is thought to occur via disassociation and evaporation in the form of free Ag atoms and O_2 with the simultaneous condensation of Ag vapor.[36] The free energy of formation of Ag_2O is approximately −11.2 kJ/mol at room temperature, with the corresponding free energy of formation per molecule being ∼0.1 eV.[34,36,37] It increases to zero at a temperature near 360 °C. The activation energy for thermal decomposition, the forward direction in reaction 3, is 120−150 kJ/mol (1.2−1.5 eV).[36] Since the bandgap of Ag_2O is near 1.3 eV, it is therefore reasonable to postulate that the reaction 3 should occur via the absorption of visible light.

Another reason to believe that Ag_2O should be photochemically active is that the reactions above are analogous with those for AgCl.[39−41] This silver halide compound decomposes via

$$AgCl + e^- \rightleftarrows Ag + Cl^- \qquad E^0 = +0.222\ V \tag{4}$$

$$AgCl \overset{light}{\rightleftharpoons} Ag + \frac{1}{2}Cl_2 \tag{5}$$

Energy levels in Figure 2 for these reactions can be plotted only approximately, since the nucleation of silver clusters increases the redox potential.[44] To test the mechanism of Figure 2 and the proposed silver oxide photochemical reduction reaction, some tests have been carried out. The results are relevant to the subsequent review of recent work on solar photochemistry and thermochemistry that utilize metal oxides. We will examine whether these chemical mechanisms can be used together synergistically.

Silver Oxide Photochemistry Setup. Silver oxide and silver chloride powders (Fluka) were reagent grade and were used without further purification. The thermogravimetry (TG)

analysis for silver oxide decomposition in darkness and under illumination was undertaken using a Netzsch Simultaneous Thermal Analysis system (Model STA 409) at a scan rate of 0.5°/min from 50 °C to 550 °C. The sample (<50 mg) was distributed on the top of an alumina pedestal that was attached to the sensitive balance of the STA 409 system. This pedestal rested on a thermocouple that provided a means for temperature measurement and control. A quartz tube allowed a Tungsten Halogen lamp to irradiate the sample from above. IR radiation was partially removed from the input beam using a Schott BG38 glass filter. A calibrated silicon detector established that the white light irradiance on the powder was in the range of 150−200 W/m^2. An air stream was used to carry away any products of decomposition. Measurements were also undertaken that determine the sample's reflectivity at a fixed wavelength as a function of temperature.[45,46] Temperature was measured by affixing a thermocouple to the Ag_2O sample. This removed the uncertainties in the temperature exhibited by the TG measurements, in which the thermocouple was some distance from the surface of the sample.

Silver Oxide Results. Figures 3 and 4 show the results of TG and differential thermogravimetry (DTG) analyses. Both

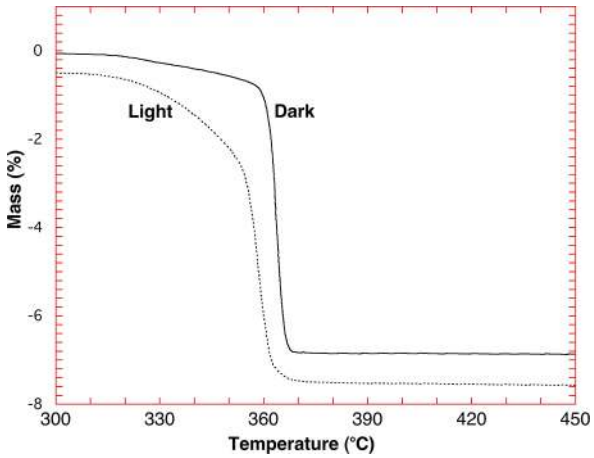

Figure 3. Thermogravimetric (TG) analysis for the silver oxide (Ag_2O) reduction reaction under illumination and in darkness. A quartz tube allowed the passage of light from a tungsten−halogen light source (150−200 W/m^2) to the oxide powder.

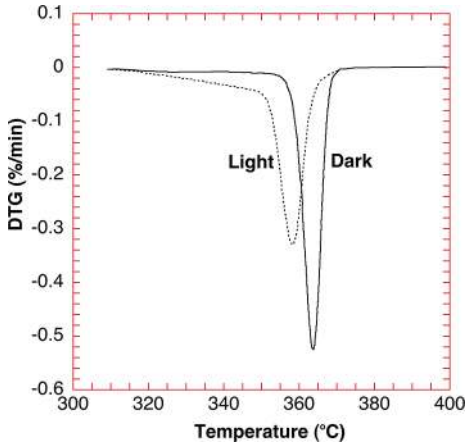

Figure 4. Differential thermogravimetry (DTG) for the thermal decomposition of Ag_2O, which represents the time derivative of the TG results from Figure 3.

for the Ag_2O sample measured in darkness and for the illuminated sample, the weight remains unchanged through most of the temperature range and then decreases very gradually beyond 250 °C (not shown on the plots). It is near this temperature that the light and dark curves diverge, with the illuminated Ag_2O sample losing as much as 0.25% in weight by the time 300 °C is reached (see Figure 3). At higher temperatures, the divergence of the light and dark curves is more pronounced until an asymptotic decrease is reached near 350−360 °C, with the transition temperature for the sample measured under illumination being ∼10 °C lower than in darkness. The Ag_2O sample in darkness exhibits a near-ideal weight loss (near 6.9%) for the reaction in reaction 3, while the curve obtained for the illuminated sample levels off beyond 7.6%.

Although reaction 3 proceeds in darkness at elevated temperatures, it does not proceed at appreciable rates under illumination at room temperature or at temperatures of <250 °C. As is shown in Figures 3 and 4, there is, however, an ∼10 °C shift to lower temperatures under illumination. This may merely be due to a heating effect of the light and the difference between the surface and thermocouple temperatures. The shift in the temperature in Figures 3 and 4 was not observed using an experimental setup that measured the Ag_2O surface temperature using a pyranometer. The reflectivity results also indicated that Ag_2O does not seem to strongly react photochemically at elevated temperatures. The reflectivity value at visible wavelengths went from 10% to 60% at a temperature of ∼360 °C, regardless of whether the sample was illuminated.

The TG, DTG, and reflectivity measurements do not positively identify that there is a strong effect from photochemistry that occurs during the thermochemical decomposition of Ag_2O in air. In contrast with Ag_2O, AgCl was observed to react photochemically at room temperature to produce reduced silver. Application of heat accelerated the reaction so that it was complete (at ∼1% weight loss) at temperatures of <100 °C. One would expect that both Ag_2O and AgCl would react photochemically in an analogous way. One reason why Ag_2O does not significantly react photochemically in air may involve the back reaction shown in Figures 1 and 2. Silver and Cl_2 diffusion in AgCl may be more rapid than Ag and O_2 diffusion in Ag_2O, and this may result in longer times for energy-dissipating reactions to occur.[34,43,44] Nonradiative recombination at defects and at the surface of the oxide could also effectively counter the accumulation of charge carriers created via light excitation. This is thought to be the case for one elevated temperature study of ZnO particles under irradiation by light.[47] Other researchers studying carbon gasification using CO_2 at high temperatures have proposed a photocatalytic effect on ZnO in addition to thermochemical processes.[48] This leaves some uncertainty as to whether a metal oxide system can be designed that can efficiently store solar energy using both thermochemical and photochemical mechanisms.

Further tests are required to determine if there are subtle enhancements in Ag_2O thermal decomposition, in air, while it is illuminated. As reported previously, Ag_2O can react photochemically in aqueous solution near room temperature.[33] The results that have been presented demonstrate that the energetics shown in Figures 1 and 2 do not solely determine the viability of a photochemical reaction for use in solar conversion. One can utilize the previously described theoretical

framework to gain insights on this assertion. From eqs 1a and 1b, we know that a difference in the concentration of electrons and holes can develop under illumination, only to be dissipated by entropy production (i.e., via recombination of charge carriers and back reactions enhanced by slow kinetics). Mathematically, $T_0\dot{S}_{tot}$ is likely to decrease the power output of a quantum solar converter as T_0 increases. In addition, the reversible work ($\dot{W}_{rev}$) decreases with increasing temperatures. Therefore, the theoretical framework and the model systems Ag_2O and AgCl both illustrate the difficulty in putting together a practical metal oxide system that might convert solar energy into fuels simultaneously, using both photochemistry and thermochemistry. These two modes of operation may conflict with each other unless special conditions are employed. Therefore, we turn our attention to purely photochemical, and then purely thermochemical, schemes for the production of fuels from sunlight.

Photochemistry and Photocatalysis for Fuels. Titanium dioxide (TiO_2) has long been known as an efficient photocatalyst, being stable in the presence of water and oxygen over a wide pH range. This allows it to split water, producing hydrogen and oxygen gas, under irradiation when it is biased with an external voltage sufficient to allow its Fermi level to rise above the redox potential for the H^+/H_2 redox couple.[11,49,50] One can understand the energetics of this reaction from Figure 1 if one highlights the fact that the upper level (UL) is the conduction band (CB) for semiconducting TiO_2, and the lower level (LL) is the valence band (VB). Without bias, the CB for TiO_2 is, unfortunately, located below the acceptor level, A (i.e., the redox couple for hydrogen). This is the case for many oxide semiconductors that have been studied for photochemical water splitting or CO_2 reduction.[9−12] To add an electron to the acceptor, which reduces it, extra energy is needed to move the chemical potential (i.e., the Fermi level) of the metal oxide above the acceptor level. This is one factor that limits the efficiency of metal oxide materials employed as photocatalysts for water splitting and CO_2 reduction.[9−12] It should be pointed out that the redox potential for hydrogen is close to that of many of the CO_2 reduction reactions, so the same challenges present themselves for both fuel-forming reactions.[127]

Another limitation of metal oxides for solar fuel production is their large bandgap (e.g., ∼3 eV for TiO_2), resulting in a poor utilization of the solar spectrum and a low solar energy conversion efficiency (at present, $\eta_{solar\text{-}to\text{-}fuel} < 2\%$ for AM1.5 irradiation).[9,11,12,51] Another challenge is in the separation and collection of the hydrogen and oxygen gas produced by the reaction, which often are in close proximity. Applying Figure 1 to water splitting, D is equal to H_2O and the oxidized product (O_2) must be kept from a backward reaction with the H_2.

Because they can be tailored for bandgap and surface properties, nanoparticle catalysts have dominated research and development (R&D) on fuel production via solar photochemistry and photocatalysis.[9,10] Utilizing thin films of hollow TiO_2 rods and tubes has resulted in higher solar conversion efficiencies with better possibilities for the separation of hydrogen and oxygen.[11,50] The photocatalytic production of H_2 from the photoreforming of alcohols has recently been shown to be up to an order of magnitude higher when compared to the water splitting process.[54] This is because TiO_2 and other metal oxides are efficient at breaking down organic compounds. This is a disadvantage when one wants to combine them with organic dyes and sensitizers to extend their useful range into the visible part of the solar spectrum. A result of this effect is that oxides like TiO_2 and ZnO have found practical uses in the photochemical detoxification of hazardous organic wastes and for the decontamination of surfaces.[53,55,56]

Recent progress in water splitting was highlighted in a review by Maeda[9] and in the overview of recent advances using a variety of oxide semiconductors.[12] Relevant to the prior discussion on Ag_2O, it has been found that improved photocatalysis is obtained from Ag/ZnO composites for which the catalytic surface properties, doping, charge carrier concentrations, and charge carrier mobilities can be more precisely controlled.[52,53] A review of more-complex semiconducting oxides discussed their use for the conversion of solar energy into chemical fuels.[57] Specifically, $AgNbO_3$, $PbTiO_3$, and $CuNbO_3$ (with bandgaps in the range of 3.2−2.0 eV) have emerged as promising metal oxide photocatalysts. While the optimum single-bandgap value for the most efficient use of the AM1.5 solar spectrum is ∼1.4 eV, this increases to ∼1.6−2.2 eV when overpotentials and kinetics are considered. The search for novel oxide materials for solar photochemistry is driven by this realization and an increasing ability to understand the correlation between an oxide's electronic structure and the energetics necessary to reduce CO_2 or to split water to form H_2.

Oxides are also proving to be useful as the electrocatalysts necessary to produce O_2. Ordinarily, it is necessary to deposit small islands of rare or expensive metals (i.e., critical materials like Pt, Pd, Ni, or Ru) on the surface of the metal oxide to provide a catalytic site for the redox reaction to occur. A molecular manganese complex inspired by natural photosynthesis has, however, been successfully employed in a photoelectrochemical cell. Here, a ruthenium bipyridyl organometallic complex, a Ru(bipy) dye, is the light absorber that transfers electrons to a porous TiO_2 film (the primary electron acceptor), where they travel through an external circuit to a cathode to evolve O_2 at the manganese oxide complex.[58] Quantum efficiencies are <2%, and the photocurrent densities are in the microamp per square centimeter ($\mu A/cm^2$) range. Still, combining knowledge from biology with improvements in the understanding of the relationship between electronic structure and catalytic activity may open up new possibilities for rationally designed photocatalysts to produce fuels from sunlight. In addition to this capability, combinatorial techniques have proven useful for the identification of oxides and mixtures of oxides for photoelectrolysis and photochemistry.[59]

Aluminosilicate zeolites have also shown promise, allowing for enhanced charge separation and excited-state lifetime.[60,63] These oxide cages can hold the donor and acceptor (shown in Figure 1) at a fixed and controllable distance that is analogous to the way that the photosystems are arranged in natural photosynthesis. Early work by Calzaferri and co-workers utilized silver as the sensitizer and light absorber trapped within the zeolite cage.[40] One of the limitations of any nanoparticle photocatalyst is surface and interface recombination. Strategies for mitigating recombination and passivating defects in oxides are the subjects of intensive research.[61]

Nanoparticle films of TiO_2 are also utilized for another solar photochemical converter, namely, the dye-sensitized solar cell (DSSC).[9,11,21,23] Tradeoffs between its performance and stability have limited the large-scale deployment of the DSSC, especially in light of the fact that other organic photovoltaics (OPVs) have achieved similar efficiencies in a fully solid-state device.[64] However, as discussed previously, the DSSC can be coupled to oxygen- and hydrogen-evolving catalysts to produce

Table 1. Donor, Absorber, and Acceptor for Several Quantum Solar Converters Mentioned in This Review as Photochemical Systems for Solar Energy Storage[a]

quantum solar converter	donor, D	absorber	acceptor, A	reference(s)
PV solar cell	*p*-type semiconductor	*p*-type, *n*-type, or intrinsic	*n*-type semiconductor	3–7, 132–134
Ru(bipy) water splitting	O_2/H_2O	Ru(bipy) dye	TiO_2 CB, H^+/H_2	11, 23, 58
AgCl	Cl_2/Cl^-	AgCl	AgCl/Ag	40, 41
Ag_2O	lattice O	Ag_2O	Ag_2O/Ag	this work
Ag_2O	organic	Ag_2O/Ag	$O_2/H_2O/H_2O_2$	33
metal oxide H_2 production	O_2/H_2O	oxide or oxide + dye	H^+/H_2	9–11, 57, 63
metal oxide CO_2 reduction	O_2/H_2O	oxide or photocatalyst	CO_2/H_2O	61, 127, 128
organic dye H_2 production	O_2/H_2O	polyoxometallates	H^+/H_2	62

[a]This should be used in conjunction with Figure 1.

fuels.[58] More-complex ruthenium bipyridyl complexes, called polyoxometallates, have also been used with metal oxides recently to split water.[62]

Table 1 and Figure 1, together with eqs 1a and 1b, are useful for conceptualizing recent advancements in various types of photochemical systems. The next section describes metal oxide systems that can be utilized thermochemically to produce fuels from concentrated sunlight. The reaction involved in these systems resembles the Ag_2O thermal decomposition and metal reduction discussed previously.

Solar Thermochemical Production. The solar thermochemical production of fuels uses concentrated solar radiation as the energy source of high-temperature heat to drive highly endothermic reactions.[1] Solar thermochemical approaches inherently operate at high temperatures and utilize the entire solar spectrum and, as such, provide thermodynamically favorable paths to efficient solar fuel production. Concentrating solar technologies—currently applied commercially for large-scale (MW) power generation—when coupled to high-temperature thermochemical reactors have the potential of reaching high solar-to-fuel energy conversion efficiencies and, consequently, producing solar fuels at large scale and at competitive costs.

Solar flux concentration ratios exceeding 2000 suns (1 sun = 1 kW/m^2) are attainable with large-scale solar tower and dish systems, and higher concentrations are possible with the incorporation of secondary optics in tandem with the primary concentrating systems (e.g., compound parabolic concentrators).[65] Such high solar radiation fluxes allow the conversion of solar energy to thermal reservoirs at 1500 K and above, which are needed for the thermochemical processes. Solar tower systems use a field of sun-tracking heliostats that focus the sun's rays onto a solar receiver mounted on top of a centrally located tower. The Cassegrain optical configuration for the tower system makes use of a hyperboloidal reflector at the top of the tower to redirect sunlight to a solar receiver located on the ground level. Solar dish systems use sun-tracking paraboloidal mirrors to focus sunlight onto a solar receiver positioned at the focus. These solar-concentrating systems have been proven to be technically feasible in large-scale commercial power plants, which are based on heating a fluid—typically air, steam, synthetic oil, helium, or molten salt—with solar energy for further use in traditional Rankine, Brayton, and Stirling heat engines.[66] Solar thermochemical applications, although not as far developed as solar thermal electricity generation, employ the same solar concentrating infrastructure with the solar reactor positioned at the focus of the solar tower (for MW centralized applications) or solar dish (for kW decentralized applications). A recent comprehensive review of the solar concentrating technologies for thermal power and thermochemical fuel production is given in ref 66.

The single-step thermal dissociation of H_2O or CO_2, known as solar thermolysis, although conceptually simple, has been impeded by the need to operate at temperatures above 2500 K for achieving a reasonable degree of dissociation, and by the need of effective techniques for separating H_2 and O_2 or CO and O_2 at high temperatures to avoid ending up with an explosive mixture. Among the ideas investigated were solar-heated semipermeable membranes made of ZrO_2 and other ceramic materials, followed by effusion, electrolytic, or de Laval nozzle separation.[67−71]

Thermochemical cycles bypass the fuel/O_2 separation problem and further allow operation at relatively moderate upper temperatures. Previous studies performed on H_2O-splitting thermochemical cycles were mostly characterized by the use of process heat at temperatures below ~1000 K, available from nuclear and other thermal sources.[72] These cycles required multiple steps (>2) and were suffering from inherent inefficiencies associated with heat transfer and product separation at each step. In contrast, solar process heat at 1500 K and above enables the more-efficient two-step thermochemical cycles using metal oxide redox reactions.[73−78] The H_2O/CO_2-splitting thermochemical cycle is shown schematically in Figure 5 and can be represented by

1st step: reduction

$$MO_{ox} \rightarrow MO_{red} + \frac{1}{2}O_2 \quad (6)$$

2nd step: oxidation

$$MO_{red} + H_2O \rightarrow MO_{ox} + H_2 \quad (7a)$$

$$MO_{red} + CO_2 \rightarrow MO_{ox} + CO \quad (7b)$$

The first endothermic step is the solar thermal reduction of the metal oxide MO_{ox} to the metal or the lower-valence metal oxide MO_{red}. The second, nonsolar, exothermic step is the oxidation of the reduced metal oxide with H_2O and/or CO_2 to form H_2 and/or CO. The reoxidized metal oxide is recycled to the first step. The net reactions are $H_2O \rightarrow H_2 + {}^1/_2O_2$ and $CO_2 \rightarrow CO + {}^1/_2O_2$. Since O_2 and fuel (H_2, CO) are released in separate steps, the need for high-temperature gas separation is thereby eliminated. The syngas mixture of H_2 and CO can be further processed to liquid hydrocarbon fuels (via Fischer–Tropsch and other catalytic processes), such as diesel, kerosene, methanol, and gasoline, using existing conventional technologies. The second step can be accomplished on demand at the fuel consumer site, because it is exothermic and decoupled from the availability of solar energy.

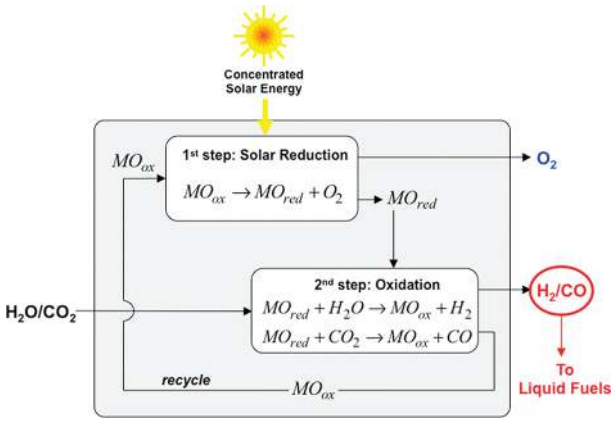

Figure 5. Schematic of a two-step solar thermochemical cycle for H_2O/CO_2 splitting based on metal oxide redox reactions.[73] MO_{ox} denotes a metal oxide, and MO_{red} represents the corresponding reduced metal oxide. In the first endothermic solar step, MO_{ox} is thermally dissociated to MO_{red} and oxygen. Concentrated solar radiation is the energy source for the required high-temperature process heat. In the second step, MO_{red} reacts with H_2O/CO_2 to produce H_2/CO (syngas). The resulting MO_{ox} is then recycled to the first step, while syngas is further processed to liquid hydrocarbon fuels.

The measure of how well solar energy is converted to chemical energy of the fuel for a given redox cycle is the solar-to-fuel energy conversion efficiency ($\eta_{\text{solar-to-fuel}}$), defined as

$$\eta_{\text{solar-to-fuel}} = \frac{-\Delta G^{\circ} \dot{n}_{\text{fuel}}}{Q_{\text{solar}}} \tag{8}$$

where Q_{solar} is the solar energy input (in watts), $\dot{n}_{\text{fuel}}$ is the molar rate of fuel production (in units of mol/s), and ΔG° is the standard Gibbs free energy of the complete oxidation of the fuel (in J/mol), i.e., the maximum amount of work that may be extracted from the fuel produced under standard temperature and pressure (STP) conditions. Note that $\eta_{\text{solar-to-fuel}}$ is often reported based on ΔH instead of ΔG, i.e., based on the high heating value (HHV) of the fuel produced; the corresponding factor should be applied when comparing with the efficiency defined by eq 8.

Among candidate redox materials, ferrite-based and analogous "non-volatile" oxides exhibit relatively slow reaction rates, a degradation in reaction rates due to sintering, and losses due to uncontrolled sublimation, whereas ZnO, SnO_2, and analogous "volatile" oxides that sublime during decomposition require rapid quenching of gaseous products to avoid recombination. One promising volatile redox system is ZnO/Zn, for which the theoretical maximum $\eta_{\text{solar-to-fuel}}$ value is equal to 35%−50%, depending on the level of heat recovery.[79−82] The ZnO dissociation proceeds at reasonable rates above 2000 K and 1 bar, while the products $Zn(g)$ and O_2 must be quenched or separated at high temperatures to avoid their recombination.[83,84] Various solar reactor concepts were examined experimentally, including entrained flows,[85] packed beds,[86] and rotating cavity receivers.[87−89] The second step of the cycle (reactions 7a and 7b) has been demonstrated using an

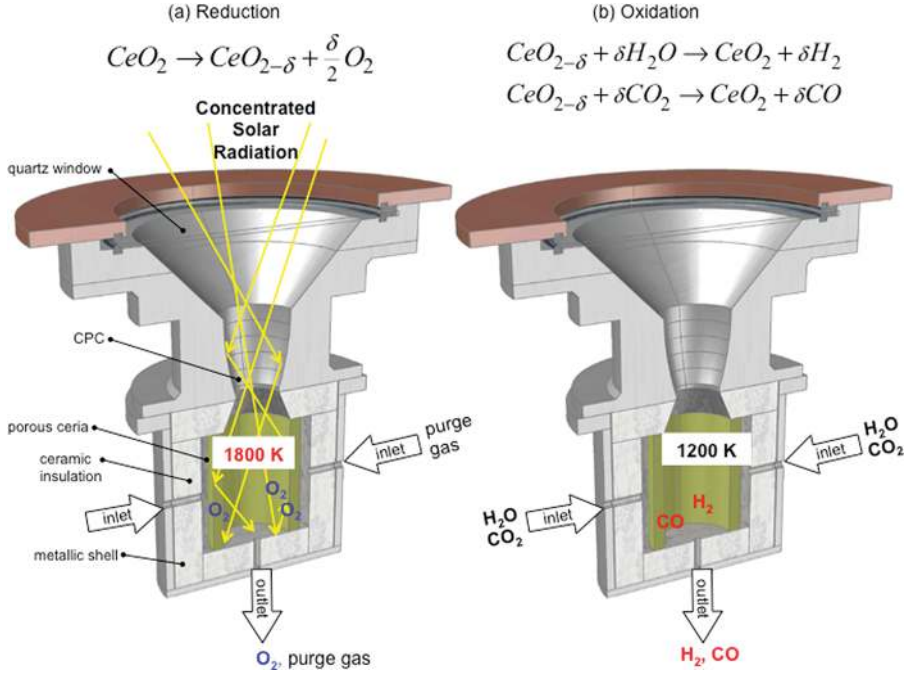

Figure 6. Scheme of the solar reactor for the $CeO_2/CeO_{2-\delta}$ redox solar thermochemical cycle.[121] It consists of a solar cavity receiver containing a porous ceria cylinder that is directly exposed to high-flux solar irradiation entering through a windowed aperture. This concept enables efficient solar absorption through multiple internal reflections and heat transfer directly to the reaction site. Reacting gases flow radially across the porous ceria, while product gases exit the cavity through an axial outlet port. During the solar, endothermic reduction 1st step (panel (a)), ceria is reduced at temperatures above ~1800 K and 1 bar via the formation of oxygen vacancies and the release of gaseous O_2, resulting in the subsequent change in stoichiometry (δ). During the nonsolar, exothermic oxidation 2nd step (panel (b)), the reduced ceria reacts with H_2O and/or CO_2 at temperatures below ~1200 K via the reincorporation of oxygen into the lattice and the release of H_2 and/or CO. The net reactions are $H_2O \rightarrow H_2 + {}^1/_2O_2$ and $CO_2 \rightarrow CO + {}^1/_2O_2$. In contrast to the direct thermolysis, fuel and O_2 are derived in different steps, thereby eliminating the need for high-temperature separation.

aerosol flow reactor for the in situ formation of Zn nanoparticles and oxidation with H_2O[90−95] and CO_2.[96] The high specific surface area of nanoparticles led to high Zn-to-ZnO conversions over short residence times due to augmented reaction kinetics and heat/mass transfer. However, the reactions primarily occurred heterogeneously outside the aerosol jet flow on surfaces with Zn deposition, making ZnO recovery problematic. Laboratory studies were also performed with steam bubbling through molten zinc,[97] but such a concept requires continuous ZnO(s) skimming. Given the aforementioned limitations, fixed-bed reactors have been explored with the aim of maximizing both Zn conversions and ZnO recovery while alleviating some of the process technology issues associated with control and scaleup.[98,99] Relatively slow kinetics due to sintering and limited mass transfer are major challenges in packed beds.[100] Analogous to the ZnO/Zn redox system, the volatile SnO_2/SnO pair is characterized by the formation of SnO in the vapor phase during the solar reduction step.[101]

A nonvolatile redox system extensively investigated is Fe_3O_4/FeO,[81,82,102−104] which requires upper operating temperatures similar to those for the ZnO/Zn system, but without undergoing sublimation. For CO_2 splitting, $\eta_{solar\text{-}to\text{-}fuel}$ = 29%, assuming no heat recovery during the quenching of products.[82] Spinel ferrites of the form $M_xFe_{3-x}O_4$ (where M generally represents Ni, Zn, Co, Mn, or other transition metals) have been shown to be capable of splitting water at moderate—and more workable—upper operating temperatures.[105−111] The drawbacks are associated with the need to provide an inert gas or vacuum pressures to drive the metal oxide reduction, which translates into an energy penalty, as well as the relatively small fraction of oxygen per unit weight of metal oxide liberated during the reduction, which introduces a scale-up limitation and imposes the need to recover sensible heat between the redox steps for achieving acceptable $\eta_{solar\text{-}to\text{-}fuel}$. The solar reactor concepts tested include ferrite-coated monoliths,[112,113] circulating fluidized beds,[114] and rotating disks.[115,116] The latter design concept utilizes two sets of beds of ferrite reactant materials in close proximity and rotating in opposite directions for thermal recuperation. Test operation of a 100-kW pilot plant based on a ferrite-based redox cycle was carried out using a monolith reactor at the solar tower of the Plataforma Solar de Almería.[117]

Ceria-based oxides have emerged as attractive nonvolatile redox candidates, because it displays faster kinetics and better stability and selectivity, relative to the ferrite-based oxides.[118−120] Figure 6 shows a solar chemical reactor configuration for performing both steps of the $CeO_2/CeO_{2-\delta}$ cycle.[121] The simultaneous splitting of H_2O and CO_2 was experimentally shown in consecutive cycles, yielding syngas with a H_2:CO molar ratio that can be controlled by adjusting the H_2O:CO_2 molar ratio in the reacting gas.[122] For example, H_2:CO = 1.7−2 would be suitable for the processing to liquid hydrocarbon fuels (e.g., diesel, kerosene) via Fischer−Tropsch synthesis. For Q_{solar} = 3 kW, the experimental measured $\eta_{solar\text{-}to\text{-}fuel}$ value was 0.8% (based on the HHV of the fuel produced), but no attempt was yet undertaken to optimize the solar reactor for maximum efficiency.[121] Both the efficiency and the cycling rates in the reactor were limited largely by thermal losses, resulting from poor conductive and radiative heat transfer across the porous ceria structure. A thermodynamic analysis indicates the potential of reaching $\eta_{solar\text{-}to\text{-}fuel}$ = 20% in the absence of heat recovery, and exceeding 30% by recovering the sensible heat of the hot products.[123] A recent techno-economic analysis for the production of methanol from H_2O and CO_2 via solar thermochemical redox cycles indicates that, with $\eta_{solar\text{-}to\text{-}fuel}$ approaching 20% (for a solar reactor mounted on a solar dish concentrator) and an overall system efficiency from solar to methanol of 7.1%, the methanol price would reach a break-even point and competitiveness vis-à-vis other renewable-resource-based alternatives.[124]

Comparison to Other Solar-to-Fuel Conversion Systems. It is useful to discuss the types of systems reviewed in this paper and to compare them to alternatives for the production of fuels from sunlight. One of the primary indicators used to compare approaches is the solar-to-fuel energy conversion efficiency, $\eta_{solar\text{-}to\text{-}fuel}$, defined by eq 8. Comparisons between thermochemical, electrolytic, photoelectrolytic, and photochemical solar-to-fuel production technologies have been made.[125] Each approach has benefits and drawbacks that can help to set future priorities for the development of thermochemical and photochemical conversion systems.

Water electrolysis powered by solar generated electricity is currently more mature than other solar-to-fuel technologies. Photovoltaic and solar thermal electricity technologies are evidently much more developed compared to other schemes for harnessing solar energy. In the former, solar cells directly convert sunlight into electricity, while in the latter—known as Concentrating Solar Power (CSP)—solar receivers absorb concentrated solar radiation to generate steam for driving a Rankine-based heat engine. CSP further allows integration of thermal storage and hybridization with fossil-fuel backup for round-the-clock electric power dispatchability.[66] Both PV and CSP technologies can be integrated with a water electrolyzer subsystem in centralized (MW) or decentralized (kW) configurations. The net product is H_2, which can be utilized by itself as a fuel or combined with CO_2 for processing liquid hydrocarbon fuels.

Assuming an electricity-to-H_2 efficiency in the range of 65%−75% for the water electrolysis step, the theoretical $\eta_{solar\text{-}to\text{-}fuel}$ value for water electrolysis-based solar-to-fuel systems can approach 30%.[11] For PV-powered water electrolysis, $\eta_{solar\text{-}to\text{-}fuel}$ = 7%−10% is expected for typical PV efficiencies near 15%. Conibeer and Richards[132] reported that, using high-efficiency multijunction solar cells based on Group III−V elements, solar-to-H_2 efficiencies of 15% were achievable. Using Group III−V materials ($Ga_{0.35}In_{0.65}P$−$Ga_{0.83}In_{0.17}As$ dual-junction solar cells), an outdoor measured solar-to-H_2 conversion efficiency of 18% has been achieved for a 96-cm^2 prototype system with a polymer electrolyte membrane electrolyzer.[133] Using standard crystalline silicon PV modules, researchers have investigated an experimental system for the production of H_2 at 415 bar (with no mechanical compressor) suitable to refuel a fuel-cell-based automobile.[134] For the combined PV−electrolyzer system, the $\eta_{solar\text{-}to\text{-}fuel}$ value approached 10%, which resulted from a PV efficiency of 15.2% and an electrolyzer efficiency of 60.3% at the intersection of their current−voltage curves.

The advantages of photoelectrochemical (photoelectrolytic) and photochemical systems include the assertion that they have fewer parts and are theoretically less likely to fail, if the remaining parts are reliable. In the former, two or more catalytic electrodes are connected to drive electrochemical reactions when they are exposed to sunlight. In this way, a separate electrolyzer is unnecessary and the electrical and electrochemical portions of water electrolysis (or, alternatively, CO_2 reduction) are combined. In purely photochemical systems, the redox reactions can take place on small particles

and unconnected surfaces. These types of schemes are simpler in design than solar/electrolyzer systems, requiring no external or internal wiring.

Equations 1a and 1b and Figure 1 apply both to PV−electrolyzer systems and to photochemical/photoelectrochemical schemes. The former can be thought of as an electrochemical system biased by an external solar cell, while the latter can be thought of as being driven by an internal solar cell (i.e., the light absorber). Note that, for photochemical and photoelectrochemical processing, the numerator of eq 8 is limited to $\dot{n}(\mu_A - \mu_D)$, as defined in eqs 1a and 1b. The difference in chemical potentials drives the fuel-forming reaction (at $-\Delta G^\circ$) that stores energy.

To determine the value of $\eta_{\text{solar-to-fuel}}$ from an experimental standpoint, an efficiency loss must be included to account for any voltage biasing necessary to bring the energy levels into proper alignment (see Figure 1). The reaction may also not produce fuel in its standard state (i.e., a pressure of 1 bar). Incorporating these aspects into eq 8, one obtains[11,126]

$$\eta_{\text{solar-to-fuel}} = \frac{-[\Delta G^\circ + RT \ln(P^\circ/P)]\dot{n}_{\text{fuel}} - V_{\text{bias}} I}{Q_{\text{solar}}} \quad (9)$$

where P is the partial pressure of the fuel produced and V_{bias} and I are, respectively, the voltage (in volts) and current (in amperes) necessary to bias the electrode. R is the molar gas constant (8.314 J K^{-1} mol^{-1}) and T is the absolute temperature. While the first two terms in the numerator are relevant for both thermochemical, photochemical, and photoelectrolysis systems, the bias term is not utilized for the purely thermochemical cycles described previously.

A typical experimental oxide-based photochemical system might produce H_2 (ΔG° = −237.2 kJ/mol) at a rate on the order of 1−100 μmol per hour per gram of catalyst. Oxide photocatalysts are frequently used at 10−100 g/m^2. Bias voltages in the range of 0.1−0.5 V are often necessary, and currents are in the range of 1−10 mA. Given 1000 W/m^2 for AM1.5 sunlight, this would yield a $\eta_{\text{solar-to-fuel}}$ value of 10^{-3}−10^{-5} (0.001%−0.1%). Using oriented TiO_2 nanotubes, efficiencies approaching 10% have been reported for irradiation by UV lamps, but were <0.5% for full spectrum illumination (AM1.5 sunlight).[11,50] Metal-oxide-based water-splitting schemes requiring biasing, either by connecting to a standard PV cell or using a chemical bias, yield solar conversion efficiencies of 0.5%−4%, depending on the light source used and how $\eta_{\text{solar-to-fuel}}$ is reported.[9,11,16,57]

A specific example comes from the photocatalytic CO_2 reduction using titanium dioxide (TiO_2) unbiased by an external voltage.[128] Substrates included both glass and flexible plastics. Isotopically labeled $^{13}CO_2$ reduction rates of 0.34 μmol h^{-1} m^{-2} were observed using an ultraviolet (UV) lamp, but it is expected that the system would only be able to produce 2.1 μmol m^{-2} per year under natural sunlight. Clearly, there is much room for efficiency improvements in photochemical and photoelectrochemical fuel-forming systems, and clear protocols for efficiency reporting will be of paramount importance as further advancements are made.

Hydrogen production from H_2O via solar thermochemical cycles is potentially more efficient and, consequently, thought to be less costly than using solar electricity to electrolyze water. Furthermore, the same solar reactor technology can be applied to produce CO from CO_2. The syngas mixture of H_2 and CO can be further processed to liquid hydrocarbon fuels using conventional catalytic processes. For the solar thermochemical approach, theoretical $\eta_{\text{solar-to-fuel}}$ values exceeding 30% are often assumed, whereas for photoelectrolysis, the expected values are <15% and those for photochemistry are <5%. Solar-to-fuel systems with overall energy efficiencies above 20% can compete with the two-stage electrolysis-based systems described in this section. This, of course, depends on the scale of the installation and its economics. For example, a theoretical economic comparison between solar H_2 generation by means of thermochemical redox cycles and electrolysis has been performed using 50 MW_{th}-scale concentrated solar thermal technologies.[129] Hydrogen production costs ranging from 3.5−12.8 €/kg for the thermochemical cycle and 2.1−6.8 €/kg for electrolysis were obtained. A comparative assessment of solar H_2 production considered either CSP with thermal storage or PV with electrical storage to power a water electrolyzer.[130] The overall efficiency of the CSP pathway was found to be double that for PV, mainly due to the thermodynamics at higher temperatures.

In the STEP (Solar Thermal Electrochemical Photo) system for H_2 production, a PV subsystem provides the voltage for a high-temperature electrolyzer, and the sunlight unused by the PV portion provides the heat.[131] An economic assessment yielded a H_2 cost of $3/kg for $\eta_{\text{solar-to-fuel}}$ = 14%. For this scheme, eqs 1a and 1b describe the limits for the PV portion, but the effect of higher temperatures on the electrolyzer stage is decoupled from that subsystem for this hybrid system.

■ CONCLUSIONS

The processes and materials for the production of solar fuels and industrial feedstocks are diverse and often difficult to interrelate. Solar photochemistry involves reactions in which the conversion of solar energy into work can proceed directly without the need to convert light into heat. Solar cells can be thought of as a photochemical reaction between photons and semiconductor materials. Photochemical approaches utilizing semiconducting metal oxides currently suffer from low absorption and utilization of the solar spectrum and high recombination rates for the products of photoexcitation prior to their separation and collection. At the laboratory and research and development (R&D) level, comparing Ag_2O to AgCl (and to ZnO) can provide fundamental insights to design better thermochemical and photochemical systems.

Solar thermochemistry has emerged as a viable path to utilize concentrated solar technology—currently applied commercially for large-scale (MW) power generation—for the conversion of H_2O and CO_2 into H_2 and CO. This syngas mixture, in turn, can be further processed to liquid hydrocarbon fuels for the transportation sector. Solar thermochemical cycles for splitting H_2O and CO_2 via metal oxide redox reaction have favorable thermodynamics, but solar-to-fuel energy conversion efficiencies above 10% are still pending experimental demonstration with robust and scalable solar reactors. It is clear from this review that thermochemical and photochemical systems have a long way to go to achieve their full potential and thus successfully compete with alternative approaches to produce fuels from sunlight.

■ AUTHOR INFORMATION

Corresponding Author

*E-mail: inquiries@solideas.com.

Notes

The authors declare no competing financial interest.

■ ACKNOWLEDGMENTS

Financial support by the Swiss Federal Office of Energy and the Swiss National Science Foundation is gratefully acknowledged. One of the authors (G.P.S.) would like to thank Dr. W. Rehwald, A. Frei, and W. Durisch (all from the Paul Scherrer Institute, Switzerland) and Dr. Yasuo Izumi (Chiba University, Japan) for their help and encouragement. The advice and guidance of Dr. Michael Grätzel (École Polytechnique Fédérale de Lausanne) and Dr. Harald Ries are acknowledged and greatly appreciated.

■ DEDICATION

This article is dedicated to the memory of Dr. Paul Kesselring, formerly Head of the General Energy Department at the Paul Scherrer Institute, a tireless mentor of young scientists, a visionary for sustainable energy, and an ardent promoter of international collaboration on solar fuels R&D.

■ REFERENCES

(1) Steinfeld, A.; Palumbo, R. Solar Thermochemical Process Technology, *Encyclopedia of Physical Science and Technology*, Vol. *15*; Academic Press: New York, 2001; pp 237−256.

(2) Villoria, J.; Navarro Yerga, R.; Al-Zahrani, S.; Fierro, J. Photocatalytic Hydrogen Production on $Cd_{1-x}Zn_xS$ Solid Solutions under Visible Light: Influence of Thermal Treatment. *Ind. Eng. Chem. Res.* **2010**, *49*, 6854−6861.

(3) Hanket, G.; Birkmire, R.; Jackson, S.; Rocheleau, R. Roll-to-Roll Deposition of a Semiconductor Film on a Flexible Substrate for Photovoltaics: Conception to Reality. *Ind. Eng. Chem. Res.* **2009**, *48*, 5923−5933.

(4) Mukati, K.; Ogunnaike, B.; Eser, E.; Fields, S.; Birkmire, R. Scaleup of $Cu(InGa)Se_2$ Thin Film Coevaporative Physical Vapor Deposition Process, 1. Evaporation Source Model Development. *Ind. Eng. Chem. Res.* **2009**, *48*, 5975−5991.

(5) Mukati, K.; Ogunnaike, B.; Eser, E.; Fields, S.; Birkmire, R. Scaleup of $Cu(InGa)Se_2$ Thin Film Coevaporative Physical Vapor Deposition Process, 2. Evaporation Source Design. *Ind. Eng. Chem. Res.* **2009**, *48*, 5992−5999.

(6) McEvoy, A; Markvart, T.; Castañer, L. *Practical Handbook of Photovoltaics Fundamentals and Applications*; Academic Press: Oxford, U.K., 2012.

(7) Liu, J. S.; Kuan, C.; Cha, S.; Chuang, W.; Gau, G. J.; Jeng, J. Photovoltaic technology development: A perspective from patent growth analysis. *Sol. Energy Mater. Sol. Cells* **2011**, *95*, 3130−3136.

(8) Hou, Y.; Vidu, R.; Stroeve, P. Solar Energy Storage Methods. *Ind. Eng. Chem. Res.* **2011**, 8954−8964.

(9) Maeda, K. Photocatalytic water splitting using semiconductor particles: History and recent developments. *J. Photochem. Photobiol. C* **2011**, *12*, 237−268.

(10) Andrews, D. L.; Scholes, G. D.; Wiederrecht, G. P. *Comprehensive Nanoscience and Technology*; Academic Press: Amsterdam, 2011; Chapter 1.17, p 571.

(11) Grimes, C. A.; Varghese, O. K.; Ranjan, S. *Light, Water, Hydrogen*; Springer: New York, 2008.

(12) Bignozzi, C. A. *Photocatalysis*; Springer: Berlin, 2011.

(13) Ries, H.; McEvoy, A. Chemical Potential and temperature of light. *J. Photochem. Photobiol. A* **1991**, *59*, 11−18.

(14) Schick, K.; Daub, E.; Finkbeiner, S.; Würfel, P. Verification of a generalized Planck law for luminescence radiation from silicon solar cell. *Appl. Phys. A: Mater. Sci. Process.* **1992**, *54*, 109−114.

(15) Ross, R. T.; Calvin, M. Thermodynamics of Light Emission and Free-Energy Storage in Photosynthesis. *Biophys. J.* **1967**, *7*, 595−614.

(16) Archer, M.; Bolton, J. Requirements for ideal performance of photochemical and photovoltaic solar energy converters. *J. Phys. Chem.* **1990**, *94*, 8028−8036.

(17) Fingerhut, B. P.; Zinth, W.; de Vivie-Riedle, R. The detailed balance limit of photochemical energy conversion. *Phys. Chem. Chem. Phys.* **2010**, *12*, 422−432.

(18) Parrot, J. E. Thermodynamics of solar cell efficiency. *Sol. Energy Mater. Sol. Cells* **1992**, *25*, 73−85.

(19) Tiedje, T.; Yablonovitch, E.; Cody, G.; Brooks, B. Limiting efficiency of silicon solar cells. *IEEE Trans. Electron. Dev.* **1984**, *31*, 711−716.

(20) Markvart, T.; Landsberg, P. T. Thermodynamics and reciprocity of solar energy conversion. *Physica E* **2002**, *14*, 71−79.

(21) Smestad, G. P. *Optoelectronics of Solar Cells*; SPIE: Bellingham, WA, 2002.

(22) Smestad, G. Absorptivity as a predictor of the photoluminescence spectra of silicon solar cells and photosynthesis. *Sol. Energy Mater. Sol. Cells* **1995**, *38*, 57−71.

(23) Smestad, G. Testing of dye sensitized TiO_2 solar cells. II: Theoretical voltage output and photoluminescence efficiencies. *Sol. Energy Mater. Sol. Cells* **1994**, *32*, 273−288.

(24) Smestad, G.; Ries, H. Luminescence and current−voltage characteristics of solar cells and optoelectronic devices. *Sol. Energy Mater. Sol. Cells* **1992**, *25*, 51−71.

(25) Ross, R. T.; Nozik, A. J. Efficiency of hot-carrier solar energy converters. *J. Appl. Phys.* **1982**, *53*, 3813−3819.

(26) Ross, R. T.; Hsiao, T. Limits on the yield of photochemical solar energy conversion. *J. Appl. Phys.* **1977**, *48*, 4783−4386.

(27) Ross, R. T.; Collins, J. M. Efficiency of quantum-utilizing solar energy converters in the presence of recombination losses. *J. Appl. Phys.* **1980**, *51*, 4504−5408.

(28) Andresen, B.; Berry, R. S.; Ondrechen, M.; Salamon, P. Thermodynamics for Processes in Finite Time. *Acc. Chem. Res.* **1984**, *17*, 266−271.

(29) Warner, J. W.; Berry, R. S. On the thermodynamics of fuel synthesis. *J. Phys. Chem.* **1987**, *91*, 2216−2226.

(30) Dennis, P. N. J. *Photodetectors*; Plenum Press: New York, 1986.

(31) Smestad, G. P. Conversion of heat and light simultaneously using a vacuum photodiode and the thermionic and photoelectric effects. *Sol. Energy Mater. Sol. Cells* **2004**, *82*, 227−240.

(32) Condon, E. U.; Odishaw, H. *Handbook of Physics*, 2nd Edition; McGraw−Hill: San Francisco, CA, 1967.

(33) Wang, X.; Li, S.; Yu, H.; Yu, J.; Liu, S. Ag_2O as a new visible-light photocatalyst: Self-stability and high photocatalytic activity. *Chem.—Eur. J.* **2011**, *17*, 7777−7780.

(34) Keim, R. *Gmelins Handbuch der Anorganishen Chemie: Silber*; Verlag Chemie GmbH: Weinheim, Germany, 1971.

(35) Gordienko, A. B.; Zhuravlev, Y. N.; Fedorov, D. G. Band Structure and Chemical Bonding in Cu_2O and Ag_2O Oxides. *Phys. Solid State* **2007**, *49*, 223−228.

(36) L'vov, B. V. Kinetics and mechanism of thermal decomposition of silver oxide. *Thermochim. Acta* **1999**, *333*, 13−19.

(37) Herley, P. J.; Prout, E. G. The Thermal Decomposition of Silver Oxide. *J. Am. Chem. Soc.* **1960**, *82*, 1540−1543.

(38) Tjeng, L. H.; Meinders, M. B. J.; van Elp, J.; Ghijsen, J.; Sawatzky, G. A.; Johnson, R. L. Electronic structure of Ag_2O. *Phys. Rev. B* **1990**, *41*, 3190−3199.

(39) Madelung, O. *Semiconductors: Supplements and Extensions to Vol. III/17*; Landolt−Bornstein, Springer−Verlag: Berlin, 1987.

(40) Beer, R.; Calzaferri, G.; Spahni, W. Photoelectrochemical Experiment with Ag/AgCl Electrodes. *Chimia* **1988**, *42*, 134−137.

(41) Rousseau, D. L.; Leroi, G. E.; Link, G. L. Two-Photon Induced Chemical Reaction in AgCl. *J. Chem. Phys.* **1965**, *42*, 4048−4049.

(42) Jiang, Z.; Huang, S.; Qian, B. Semiconductor properties of Ag_2O film formed on the silver electrode in 1 M NaOH solution. *Electrochim. Acta* **1994**, *39*, 2465−2470.

(43) Belloni-Cofler, J.; Amblard, J.; Marignier, J.-L.; Mostafavi, M. Photography revealed: The principles of development. *Endeavor* **1991**, *15*, 2−9.

(44) Marignier, J. L.; Belloni, J.; Delcourt, M.; Chavalier, J. Microaggregates of non-noble metals and bimetallic alloys prepared by radiation-induced reduction. *Nature* **1985**, *317*, 344−345.
(45) Schubnell, M.; Tschudi, H. R.; Kuhn, P.; Ries, H. Reflectivity as a probe for chemical reactions. *J. Chem. Sci.* **1993**, *105*, 671−675.
(46) Schubnell, M.; Tschudi, H. R. Simultaneous measurement of irradiation, temperature and reflectivity on hot irradiated surfaces. *Appl. Phys. A: Mater. Sci. Process.* **1995**, *60*, 581−587.
(47) Schubnell, M.; Kamber, I.; Beaud, P. Photochemistry at high temperatures—Potential of ZnO as a high temperature photocatalyst. *Appl. Phys. A: Mater. Sci. Process.* **1997**, *64*, 109−113.
(48) Gokon, N.; Hasegawa, N.; Kaneko, H.; Aoki, H.; Tamaura, Y.; Mitsunobu, K. Photocatalytic effect of ZnO on carbon gasification with CO_2 for high temperature solar thermochemistry. *Sol. Energy Mater. Sol. Cells* **2003**, *80*, 335−341.
(49) Murphy, A. B.; Barnes, P. R. F.; Randeniya, L. K.; Plumb, I. C.; Grey, I. E.; Horne, M. D.; Glasscock, J. A. Efficiency of solar water splitting using semiconductor electrodes. *Int. J. Hydrogen Energy* **2006**, *31*, 1999−2017.
(50) Jiang, J.; Gu, F.; Shao, W.; Li, C. Fabrication of Spherical Multi-Hollow TiO_2 Nanostructures for Photoanode Film with Enhanced Light-Scattering Performance. *Ind. Eng. Chem. Res.* **2012**, *51*, 2838−2845.
(51) Fu, N.; Tang, Z.; Li, D. Is it effective to harvest visible light by decreasing the band gap of photocatalytic materials? *Appl. Phys. Lett.* **2012**, *100*, 093901.
(52) Zhang, Y.; Mu, J. One-pot synthesis, photoluminescence, and photocatalysis of Ag/ZnO composites. *J. Colloid Interface Sci.* **2007**, *309*, 478−484.
(53) Ahn, B. D.; Kang, H. S.; Kim, H. J.; Kim, G. H.; Change, H. W.; Lee, S. Y. Synthesis and analysis of Ag-doped ZnO. *J. Appl. Phys.* **2006**, *100*, 093701.
(54) Seferlis, A. K.; Neophytides, S. G. Photoelectrocatalytic Electricity and/or H_2 Production from Alcohols: The Effect of TiO_2 Film Thickness. *J. Electrochem. Soc.* **2011**, *158*, H183−H189.
(55) Medina-Valtierra, J.; Frausto-Reyes, C.; Ramírez-Ortiz, J.; Camarillo-Martínez, G. Self-Cleaning Test of Doped TiO_2-Coated Glass Plates under Solar Exposure. *Ind. Eng. Chem. Res.* **2009**, *48*, 598−606.
(56) Augugliaro, V.; Loddo, V.; Palmisano, G.; Palmisano, L, Pagliaro, M. *Clean by Light Irradiation*; RSC Publishing: Cambridge, U.K., 2010.
(57) Joshi, U. A.; Palasyuk, A.; Arney, D.; Maggard, P. A. Semiconducting Oxides to Facilitate the Conversion of Solar Energy to Chemical Fuels. *J. Phys. Chem. Lett.* **2010**, *1*, 2719−2726.
(58) Brimblecombe, R.; Koo, A.; Dismukes, G. C.; Swiegers, G. F.; Spiccia, L. Solar Driven Water Oxidation by a Bioinspired Manganese Molecular Catalyst. *J. Am. Chem.* **2010**, *132*, 2892−2894.
(59) Woodhouse, M.; Parkinson, B. A. Combinatorial approaches for the identification and optimization of oxide semiconductors for efficient solar photoelectrolysis. *Chem. Soc. Rev.* **2009**, *38*, 197−210.
(60) Dutta, P. K.; Severance, M. Photoelectron Transfer in Zeolite Cages and Its Relevance to Solar Energy Conversion. *J. Phys. Chem. Lett.* **2011**, *2*, 467−476.
(61) He, H.; Liu, C.; Dubois, K. D.; Jin, T.; Louis, M. E.; Li, G. Enhanced Charge Separation in Nanostructured TiO_2 Materials for Photocatalytic and Photovoltaic Applications. *Ind. Eng. Chem. Res.* **2012**, in press (DOI: 10.1021/ie300510n).
(62) Huang, Z.; Geletii, Y. V.; Musaev, D. G.; Hill, C. L.; Lian, T. Spectroscopic Studies of Light-driven Water Oxidation Catalyzed by Polyoxometalates. *Ind. Eng. Chem. Res.* **2012**, in press (DOI: 10.1021/ie202950h).
(63) Ryu, S.; Choi, J.; Balcerski, W.; Lee, T.; Hoffmann, M. Photocatalytic Production of H_2 on Nanocomposite Catalysts. *Ind. Eng. Chem. Res.* **2007**, *46*, 7476−7488.
(64) Krebs, F. C. *Polymeric Solar Cells*; Destech Publications, Inc.: Lancaster, PA, 2010.
(65) Welford, W. T.; Winston, R. *High Collection Nonimaging Optics*; Academic Press: San Diego, CA, 1989.
(66) Romero, M.; Steinfeld, A. Concentrating Solar Thermal Power and Thermochemical Fuels. *Energy Environ. Sci.* **2012**, in press (DOI: 10.1039/C2EE21275G).
(67) Fletcher, E. A.; Moen, R. L. Hydrogen and Oxygen from Water. *Science* **1977**, *197*, 1050−1056.
(68) Kogan, A. Direct solar thermal splitting of water and on-site separation of the products—II. Experimental feasibility study. *Int. J. Hydrogen Energy* **1998**, *23*, 89−98.
(69) Fletcher, E. A. Solar thermal and solar quasi-electrolytic processing and separations: Zinc from zinc oxide as an example. *Ind. Eng. Chem. Res.* **1999**, *38*, 2275−2282.
(70) Traynor, A. J.; Jensen, R. J. Direct Solar Reduction of CO_2 to Fuel: First Prototype Results. *Ind. Eng. Chem. Res.* **2002**, *41*, 1935−1939.
(71) Karni, J.; Ferdiman, G.; Alioshin, Y. System and method for chemical potential energy production. Patent U.S. 2011/0108435 A1.
(72) Funk, J. Thermochemical hydrogen production: Past and present. *Int. J. Hydrogen Energy* **2001**, *26*, 185−190.
(73) Steinfeld, A. Solar Thermochemical Production of Hydrogen. *Solar Energy* **2005**, *78*, 603−615.
(74) Perkins, C.; Weimer, A. W. Solar-thermal production of renewable hydrogen. *AIChE J.* **2009**, *55*, 286−293.
(75) Abanades, S.; Charvin, P.; Flamant, G.; Neveu, P. Screening of water-splitting thermochemical cycles potentially attractive for hydrogen production by concentrated solar energy. *Energy* **2006**, *31*, 2805−2822.
(76) Kodama, T. High-temperature solar chemistry for converting solar heat to chemical fuels. *Prog. Energy Combust. Sci.* **2003**, *29*, 567−597.
(77) Kodama, T.; Gokon, N. Thermochemical Cycles for High-Temperature Solar Hydrogen Production. *Chem. Rev.* **2007**, *107*, 4048−4077.
(78) Service, R. F. Sunlight in Your Tank. *Science* **2009**, *326*, 1472−1475.
(79) Steinfeld, A. Solar Hydrogen Production via a Two-Step Water Splitting Thermochemical Cycle Based on Zn/ZnO Redox Reactions. *Int. J. Hydrogen Energy* **2002**, *27*, 611−619.
(80) Perkins, C.; Weimer, A. W. Likely near-term solar-thermal water splitting technologies. *Int. J. Hydrogen Energy* **2004**, *29*, 1587−1599.
(81) Charvin, P.; Abanades, S.; Lemort, F.; Flamant, G. Analysis of solar processes for hydrogen production from water-splitting thermochemical cycles. *Energy Convers. Manage.* **2008**, *49*, 1547−1556.
(82) Galvez, M. E.; Loutzenhiser, P.; Hischier, I.; Steinfeld, A. CO_2 splitting via 2-step solar thermochemical cycles with Zn/ZnO and FeO/Fe_3O_4 redox reactions—Thermodynamic analysis. *Energy Fuels* **2008**, *22*, 3544−3550.
(83) Schunk, L.; Steinfeld, A. Kinetics of the thermal dissociation of ZnO exposed to concentrated solar irradiation using a solar-driven thermogravimeter in the 1800−2100 K range. *AIChE J.* **2009**, *55*, 1497−1504.
(84) Möller, S.; Palumbo, R. Solar thermal decomposition kinetics of ZnO in the temperature range 1950−2400 K. *Chem. Eng. Sci.* **2001**, *56*, 4505−4515.
(85) Perkins, C.; Lichty, P. R.; Weimer, A. W. Thermal ZnO Dissociation in a Rapid Aerosol Reactor as part of a Solar Hydrogen Production Cycle. *Int. J. Hydrogen Energy* **2008**, *33*, 499−510.
(86) Schunk, L.; Lipinski, W.; Steinfeld, A. Ablative heat transfer in a shrinking packed-bed of ZnO undergoing solar thermal dissociation. *AIChE J.* **2009**, *55*, 1659−1666.
(87) Abanades, S.; Charvin, P.; Flamant, G. Design and simulation of a solar chemical reactor for the thermal dissociation of volatile metal oxides: case study of zinc oxide dissociation. *Chem. Eng. Sci.* **2007**, *62*, 6323−6333.
(88) Schunk, L.; Lipinski, W.; Steinfeld, A. Heat transfer model of a solar receiver-reactor for the thermal dissociation of ZnO − Experimental validation at 10 kW and scale-up to 1 MW. *Chem. Eng. J.* **2009**, *150*, 502−508.

(89) Schunk, L.; Haeberling, P.; Wepf, S.; Wuillemin, D.; Meier, A.; Steinfeld, A. A solar receiver-reactor for the thermal dissociation of zinc oxide. *J. Solar Energy Eng.* **2008**, *130*, 021009.
(90) Weiss, R.; Ly, H.; Wegener, K.; Pratsinis, S. E.; Steinfeld, A. H_2 production by Zn hydrolysis in a hot-wall aerosol reactor. *AIChE J.* **2005**, *51*, 1966−1970.
(91) Wegner, K.; Ly, H.; Weiss, R.; Pratsinis, S. E.; Steinfeld, A. In situ formation and hydrolysis of Zn nanoparticles for H_2 production by the 2-step ZnO/Zn water-splitting thermochemical cycle. *Int. J. Hydrogen Energy* **2005**, *31*, 55−61.
(92) Abu Hamed, T.; Davidson, J.; Stolzenburg, M. Hydrolysis of Evaporated Zn in a Hot Wall Flow Reactor. *J. Solar Energy Eng.* **2008**, *130*, 041010−1−7.
(93) Funke, H. H.; Diaz, H.; Liang, X.; Carney, C. S.; Weimer, A. W.; Li, P. Hydrogen generation by hydrolysis of Zn powder aerosol. *Int. J. Hydrogen Energy* **2008**, *33*, 1027−1134.
(94) Ernst, F. O.; Tricoli, A.; Pratsinis, S. E.; Steinfeld, A. Co-synthesis of H_2 and ZnO by in-situ Zn aerosol formation and hydrolysis. *AIChE J.* **2006**, *52*, 3297−3303.
(95) Melchior, T.; Piatkowski, N.; Steinfeld, A. H_2 production by steam-quenching of Zn vapor in a hot-wall aerosol flow reactor. *Chem. Eng. Sci.* **2009**, *64*, 1095−1101.
(96) Loutzenhiser, P.; Galvez, E.; Hischier, I.; Graf, A.; Steinfeld, A. CO_2 splitting in an aerosol flow reactor via the two-step Zn/ZnO solar thermochemical cycle. *Chem. Eng. Sci.* **2010**, *65*, 1855−1864.
(97) Berman, A.; Epstein, M. The kinetics of hydrogen production in the oxidation of liquid zinc with water vapor. *Int. J. Hydrogen Energy* **2000**, *25*, 957−967.
(98) Loutzenhiser, P.; Barthel, F.; Stamatiou, A.; Steinfeld, A. CO_2 reduction with Zn particles in a packed-bed reactor. *AIChE J.* **2011**, *57*, 2529−2534.
(99) Stamatiou, A.; Loutzenhiser, P.; Steinfeld, A. Syngas production from H_2O and CO_2 over Zn particles in a packed-bed reactor. *AIChE J.* **2012**, *58*, 625−631.
(100) Stamatiou, A.; Loutzenhiser, P.; Steinfeld, A. Solar syngas production via H_2O/CO_2-splitting thermochemical cycles with Zn/ZnO and FeO/Fe_3O_4 redox reactions. *Chem. Mater.* **2010**, *22*, 851−859.
(101) Abanades, S.; Charvin, P.; Lemont, F.; Flamant, G. Novel two-step SnO_2/SnO water-splitting cycle for solar thermochemical production of hydrogen. *Int. J. Hydrogen Energy* **2008**, *33*, 6021−6030.
(102) Steinfeld, A.; Sanders, S.; Palumbo, R. Design Aspects of Solar Thermochemical Engineering—A case study: two-step water-splitting cycle using the Fe_3O_4/FeO redox systems. *Solar Energy* **1999**, *65*, 43−53.
(103) Charvin, P.; Abanades, S.; Flamant, G.; Lemort, F. Two-step water-splitting thermochemical cycle based on iron oxide redox pair for solar hydrogen production. *Energy* **2007**, *32*, 1124−1133.
(104) Ehrensberger, K.; Palumbo, R.; Larson, C.; Steinfeld, A. Production of Carbon from CO_2 with Iron Oxides and High-Temperature Solar Energy. *Ind. Eng. Chem. Res.* **1997**, *36*, 645−648.
(105) Tamaura, Y.; Steinfeld, A.; Kuhn, P.; Ehrensberger, K. Production of Solar Hydrogen by a Novel, 2-Step, Water-Splitting Thermochemical Cycle. *Energy* **1995**, *20*, 325−330.
(106) Fernando, F.; Fernandez-Saavedra, R.; Gomez-Mancebo, M.; Vidal, A.; Sanchez, M.; Rucandio, M.; Quejido, A.; Romero, M. Solar hydrogen production by two-step thermochemical cycles: Evaluation of the activity of commercial ferrites. *Int. J. Hydrogen Energy* **2009**, *34*, 2918−2924.
(107) Miller, J. E.; Allendorf, M. D.; Diver, R. B.; Evans, L. R.; Siegel, N. P.; Stuecker, J. N. Metal oxide composites and structures for ultra-high temperature solar thermochemical cycles. *J. Mater. Sci.* **2008**, *43*, 4714−4728.
(108) Allendorf, M. D.; Diver, R. B.; Siegel, N. P.; Miller, J. E. Two-Step Water Splitting Using Mixed-Metal Ferrites: Thermodynamic Analysis and Characterization of Synthesized Materials. *Energy Fuels* **2008**, *22*, 4115−4124.
(109) Gokon, N.; Murayama, H.; Nagasaki, A.; Kodama, T. Thermochemical two-step water splitting cycles by monoclinic ZrO_2-supported $NiFe_2O_4$ and Fe_3O_4 powders and ceramic foam devices. *Solar Energy* **2009**, *83*, 527−537.
(110) Gokon, N.; Hasegawa, T.; Takahashi, S.; Kodama, T. Thermochemical two-step water-splitting for hydrogen production using Fe-YSZ particles and a ceramic foam device. *Energy* **2008**, *33*, 1407−1416.
(111) Ishihara, H.; Kaneko, H.; Hasegawa, N.; Tamaura, Y. Two-step water-splitting at 1273−1623 K using yttria-stabalized zirconia-iron oxide solid solution via co-precipitation and solid-state reaction. *Energy* **2008**, *33*, 1788−1793.
(112) Agrafiotis, C.; Roeb, M.; Konstandopoulos, A. G.; Nalbandian, L.; Zaspalis, V. T.; Sattler, C.; Stobbe, P.; Steele, A. M. Solar Water Splitting for Hydrogen Production with Monolithic Reactors. *Solar Energy* **2005**, *79*, 409−421.
(113) Roeb, M.; Sattler, C.; Klueser, R.; Monnerie, N.; De Oliveira, L.; Konstandopoulos, A. G.; Agrafiotis, C.; Zaspalis, V.; Nalbandian, L.; Steele, A.; Stobbe, P. Solar hydrogen production by a two-step cycle based on mixed iron oxides. *J. Solar Energy Eng.* **2006**, *128*, 125−133.
(114) Gokon, N.; Takahashi, S.; Yamamoto, H.; Kodama, T. Thermochemical two-step water-splitting reactor with internally circulating fluidized bed for thermal reduction of ferrite particles. *Int. J. Hydrogen Energy* **2008**, *33*, 2189−2199.
(115) Kaneko, H.; Miura, T.; Fuse, A.; Ishihara, H.; Taku, S.; Fukuzumi, H.; Naganuma, Y.; Tamaura, Y. Rotary-Type Solar Reactor for Solar Hydrogen Production with Two-step Water Splitting Process. *Energy Fuels* **2007**, *21*, 2287−2293.
(116) Diver, R. B.; Miller, J. E.; Allendorf, M. D.; Siegel, N. P.; Hogan, R. E. Solar Thermochemical Water-Splitting Ferrite-Cycle Heat Engines. *J. Sol. Energy Eng.* **2008**, *130*, 041001.
(117) Roeb, M.; Säck, J.-P.; Rietbrock, P.; Prahl, C.; Schreiber, H.; Neises, M.; de Oliveira, L.; Graf, D.; Ebert, M.; Reinalter, W.; Meyer-Grünefeldt, M.; Sattler, C.; Lopez, A.; Vidal, A.; Elsberg, A.; Stobbe, P.; Jones, D.; Steele, A.; Lorentzou, S.; Pagkoura, C.; Zygogianni, A.; Agrafiotis, C.; Konstandopoulos, A. G. Test operation of a 100 kW pilot plant for solar hydrogen production from water on a solar tower. *Sol. Energy* **2011**, *85*, 634−644.
(118) Chueh, W. C.; Haile, S. M. Ceria as a Thermochemical Reaction Medium for Selectively Generating Syngas or Methane from H_2O and CO_2. *Chem. Sus. Chem.* **2009**, *2*, 735−739.
(119) Chueh, W. C.; Haile, S. M. A thermochemical study of ceria: exploiting an old material for new modes of energy conversion and CO_2 mitigation. *Phil. Trans. R. Soc. A* **2010**, *368*, 3269−3294.
(120) Abanades, S.; Legal, A.; Cordier, A.; Peraudeau, G.; Flamant, G.; Julbe, A. Investigation of reactive cerium-based oxides for H_2 production by thermochemical two-step water-splitting. *J. Mater. Sci.* **2010**, *45*, 4163−4173.
(121) Chueh, W. C.; Falter, C.; Abbott, M.; Scipio, D.; Furler, P.; Haile, S. M; Steinfeld, A. High-Flux Solar-Driven Thermochemical Dissociation of CO_2 and H_2O using Nonstoichiometric Ceria. *Science* **2010**, *330*, 1797−1801.
(122) Furler, P.; Scheffe, J.; Steinfeld, A. Syngas production by simultaneous splitting of H_2O and CO_2 via ceria redox reactions in a high-temperature solar reactor. *Energy Environ. Sci.* **2012**, *5*, 6098−6103.
(123) Scheffe, J.; Steinfeld, A. Thermodynamic Analysis of Cerium-based Oxides for Solar Thermochemical Fuel Production. *Energy Fuels* **2012**, *26*, 1928−1936.
(124) Kim, J.; Henao, C. A.; Johnson, T. A.; Dedrick, D. E.; Miller, J. E.; Stechel, E. B.; Maravelias, C. T. Methanol production from CO_2 using solar-thermal energy: process development and techno-economic analysis. *Energy Environ. Sci.* **2011**, *4*, 3122−3132.
(125) Wang, Z.; Roberts, R. R.; Naterer, G. F.; Gabriel, K. S. Comparison of thermochemical, electrolytic, photoelectrolytic and photochemical solar-to-hydrogen production technologies. *Int. J. Hydrogen Energy* **2012**, DOI: 10.1016/j.ijhydene.2012.03.057.
(126) Bolton, J. R. Solar photoproduction of hydrogen: A review. *Sol. Energy* **1996**, *57*, 37−50.

(127) Izumi, Y. Recent advances in the photocatalytic conversion of carbon dioxide to fuels with water and/or hydrogen using solar energy and beyond. *Coord. Chem. Rev.* **2012**, DOI: 10.1016/j.ccr.2012.04.018.
(128) Jensen, J.; Mikkelsen, M.; Krebs, F. C. Flexible substrates as basis for photocatalytic reduction of carbon dioxide. *Sol. Energy Mater. Sol. Cells* **2011**, *95*, 2949−2958.
(129) Graf, D.; Monnerie, N.; Roeb, M.; Schmitz, M.; Sattler, C. Economic comparison of solar hydrogen generation by means of thermochemical cycles and electrolysis. *Int. J. Hydrogen Energy* **2008**, *33*, 4511−4519.
(130) Joshi, A. S.; Dincer, I.; Reddy, B. V. Solar hydrogen production: A comparative performance assessment. *Int. J. Hydrogen Energy* **2011**, *36*, 11246−11257.
(131) Licht, S.; Chtayat, O.; Bergmann, H.; Dick, A.; Ayub, H.; Ghosh, S. Efficient STEP (solar thermal electrochemical photo) production of hydrogen—An economic assessment. *Int. J. Hydrogen Energy* **2010**, *35*, 10867−10882.
(132) Conibeer, G. J.; Richards, B. S. A comparison of PV/electrolyser and photoelectrolytic technologies for use in solar to hydrogen energy storage systems. *Int. J. Hydrogen Energy* **2007**, *32*, 2703−2711.
(133) Peharz, G.; Dimroth, F.; Wittstadt, U. Solar hydrogen production by water splitting with a conversion efficiency of 18%. *Int. J. Hydrogen Energy* **2007**, *32*, 3248−3252.
(134) Kelly, N. A.; Gibson, T. L.; James, M. C.; Spearot, A.; Ouwerkerk, D. B. Development of a renewable hydrogen economy: Optimization of existing technologies. *Int. J. Hydrogen Energy* **2010**, *35*, 892−899.